Performance Analysis of Synchronization Algorithms for Grid-Connected Power Converters Under Sub and Inter-Harmonics Distortion

Jean M. L. Fonseca*, Samuel S. Queiroz*, Siomara R. Lima†, Welton da Silva Lima*,
Rosana G. Almeida*, Francisco Kleber A. Lima*, and Carlos Gustavo C. Branco*
*Federal University of Ceará
Fortaleza, Brazil
Emails: jlobodaf@alu.ufc.br, samuelsqueiroz100@gmail.com,
rosana.g.a26@gmail.com, klima@dee.ufc.br, gustavo@dee.ufc.br
† Federal Institute of Education, Science and Technology of Ceará
Fortaleza, Brazil
Email: siomara.lima@ifce.edu.br

***Abstract*—This paper analyzes the performance of two synchronization algorithms, the EPLL and the ISI-PLL, under scenarios where inter-harmonics and sub-harmonics distortion are present in the input signals. Synchronization algorithms main goals are to estimate, with high accuracy, power grid parameters such as frequency and phase-angle. The EPLL is a well-known structure that is widely studied in the literature, whereas the ISI-PLL is a recent proposal. In order to obtain experimental results, both structures were implemented in the hardware-in-the-loop (HIL) dSPACE 1103 platform. Results showed that where the proposed structure is highly accurate under the considered scenarios, the EPLL estimation is not as precise.**

***Index Terms*—Phase-locked loop, Inter-harmonics, Sub-harmonics, Power Quality, Power Converters.**

I. Introduction

Power electronics devices have become very important for the modern power grid. They have several applications such as in distributed generation (i.e. photovoltaic and wind farms [1]), FACTS devices (i.e. STATCOM and UPFC [2]–[4]), active filters [5]–[7]. For the control strategies of most of these applications, information regarding the grid's voltage (and/or current) amplitude, frequency and phase-angle play a major role. Therefore, there is a demand for synchronization algorithms that are capable of estimating these parameters with high accuracy and in a fast manner.

Power supply systems are supposed to operate at a determined frequency (60 Hz in North America and Brazil or 50 Hz in Europe), however, this is not always the case. In adverse grid condition, caused by grid faults and the increased use of non-linear loads, harmonics distortion, phase-angle jump, and different sequence components are a common factor that grid-connected power converters must deal with in order to continually provide the grid with its normal functionalities.

Phase-angle jumps are caused by a change in the X/R of the system and are usually associated with voltage sags. They are thoroughly discussed in [8]. Harmonics are either integer or non-integer multiples of the power frequency. Specifically, non-integer multiples are known as inter-harmonics (sub-harmonics are inter-harmonics where the non-integer multiple is less than one). Sub and inter-harmonics can be generated, for instance, by arc furnaces/welders, cycloconverters or adjustable speed drives [9]–[12]. The presence of such distortions can cause light flicker in lighting systems, core saturation in transformers and accuracy loss in synchronization algorithms.

IEEE Std. 519-2014 recommends harmonics limits within electric power systems [13]. The maximum total integer-multiple harmonic distortion allowed at a point of common coupling (PCC) with nominal voltage less than 1 kV is 8%, with individual harmonic no greater than 5% for short time periods. These values reduce progressively as the voltage level increases. In the case of non-integer multiple harmonic distortion, the standard suggests voltage limits based on lamp flicker assessed making use of a technique presented in [14]. The range varies between 5% for frequencies very near the fundamental frequency of 60 Hz, less than 16 Hz or greater than 114 Hz. For frequencies in between, the curve varies in a parabolic-like manner from 5% to values close to 0%.

Several synchronization algorithms can be found in the literature, however, closed loop structures, such as the phase-locked loop (PLL) have obtained good results under unbalanced and distorted grid conditions [15]–[17]. Accuracy, however, becomes even trickier when input signals contain inter-harmonics close to the fundamental frequency. In such scenarios, the PLL should have an enhanced filtering capability. The aim of this paper, therefore, is to analyze the steady-state and dynamic performances of a well-known structure, the enhanced PLL (EPLL), and of a new proposal, the ISI-PLL, under sub and inter-harmonic distortion.

An overview and the mathematical modeling of the EPLL and ISI-PLL is presented in Section II. Section III shows experimental results obtained through the hardware-in-the-loop (HIL) platform DSPACE 1103 whereas Section IV has the concluding remarks of the paper.

978-1-5386-1180-7/18/$31.00 ©2018 IEEE

II. STUDIED PLL STRUCTURES

In this section the EPLL and ISI-PLL structures will be briefly presented and their mathematical models derived.

A. EPLL

The single-phase EPLL structure was proposed in [18]. The name enhanced comes from the fact that the structure removes a common problem of the conventional PLL, the double-frequency error. This is accomplished by adding a new loop to the conventional structure. Within this loop, which is illustrated inside the upper dashed-box in Figure 1, the amplitude of the input signal is estimated. The EPLL can also be seen as a non-linear adaptive notch filter and, therefore, is capable of outputting a filtered version of the input signal. This feature, in conjunction with its structural simplicity, makes it a great solution for several power systems applications [19].

From Figure 1, it is possible to derive the following governing equations for the EPLL:

$$\begin{cases} V(t) = \int e(t)\cos\theta(t)\,K dt \\ \Delta\omega(t) = \int e(t)\sin\theta(t)\,K_i dt \\ \theta(t) = \int \left[e(t)\sin\theta(t)\,K_p + \Delta\omega t + w_0\right] dt \\ e(t) = u(t) - V\cos\theta(t) \end{cases} . \quad (1)$$

Where $V(t)$, ω, θ_e, are the estimated amplitude, angular frequency and phase angle of the EPLL, respectively, and $e(t)$ is the total distortion and noise. In addition, through the use of two different trigonometric functions, the structure provides in-quadrature signals.

Lastly, the parameters K, K_p and K_i are responsible for controlling the structure's performance such the time to reach steady-state and filtering capabilities. This paper will not address how these parameters can be found however, the reader can find more information in [20].

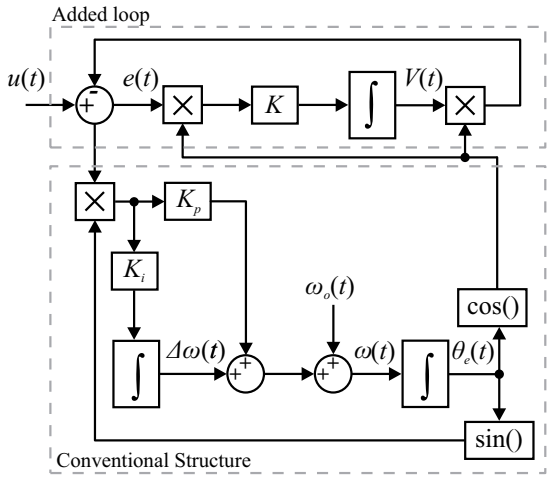

Fig. 1. Single-phase EPLL structure.

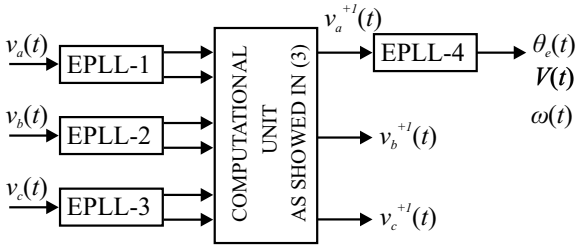

Fig. 2. Three-phase EPLL structure.

The three-phase EPLL structure was proposed in [17]. Figure 2 shows that this structure is composed by four single-phase EPLLs and a computational unit.

The structure works as follows: i) a fundamental signal for each phase, as well as a in-quadrature counter-part, is obtained making use of the filtering feature of the single-phase EPLL structure; ii) the six output signals are used as inputs for the computational unit that will extract the positive sequence components for each phase. This unit uses the Lyon transformation, a time-domain expansion for the Fortescue theorem, which says that unbalanced phasors can be represented as a combination of several balanced phasors. The transformation matrix utilized to obtain the positive sequence is shown in Equation 2.

$$\begin{bmatrix} v_a^+(t) \\ v_b^+(t) \\ v_c^+(t) \end{bmatrix} = \frac{1}{3}\begin{bmatrix} 1 & \alpha & \alpha^2 \\ \alpha^2 & 1 & \alpha \\ \alpha & \alpha^2 & 1 \end{bmatrix}\begin{bmatrix} v_a(t) \\ v_b(t) \\ v_c(t) \end{bmatrix}. \quad (2)$$

Where α is an operator that represents a $120°$ time-shift of the instantaneous input signal, that is, a time-domain equivalent of $e^{j\frac{2\pi}{3}}$. Knowing that $e^{\pm j\frac{2\pi}{3}} = \pm\frac{1}{2} \pm \frac{\sqrt{3}}{2}e^{\frac{\pi}{2}}$, Equation 2 can be rewritten as:

$$\begin{cases} v_a^{+1}(t) = \frac{1}{3}v_a^f(t) - \frac{1}{6}(v_b^f(t) + v_c^f(t)) - \\ \qquad \frac{1}{2\sqrt{3}}q(v_b^f(t) - v_c^f(t)) \\ v_b^{+1}(t) = -v_a^+(t) - v_c^+(t) \\ v_c^{+1}(t) = \frac{1}{3}v_c^f(t) - \frac{1}{6}(v_a^f(t) + v_b^f(t)) - \\ \qquad \frac{1}{2\sqrt{3}}q(v_a^f(t) - v_b^f(t)) \end{cases} . \quad (3)$$

Where q represents a 90 degrees time-domain shift and, f the fundamental component.

Finally, a fourth EPLL is used in order to estimate the phase angle, the amplitude and the angular frequency of the fundamental positive sequence voltage of one of the input phases.

Because of the multiple single-phase EPLLs and the computational unit, the three-phase EPLL algorithm is a robust structure even under polluted grid scenarios where harmonics and different sequence components are present. The structure itself is still easy to digitally implement using either DSP microcontroller or dSPACE and it does not represent a great computational burden.

B. ISI-PLL

The ISI-PLL, shown in Figure 1, is an adaptation of the structure presented in [21]. A single-phase realization of the adapted structure can be found in [22]. The following paragraphs will derive the realization of the three-phase structure for the ISI-PLL.

The PLL works as follows: two input signals on the $\alpha\beta$ reference frame are obtained from the three-phase input signals through amplitude invariant Clarke's Transformation. These signals, $\vec{v}_{\alpha\beta}$, can be projected onto a complex sub-space on the $\alpha\beta$ reference plane, $e^{-j(2\pi\hat{f}_1 t)_{\alpha\beta}}$, through the inner product defined as $\vec{g}_{\alpha\beta}(t) = \langle e^{-(j2\pi\hat{f}_1 t)_{2\phi}}, \vec{v}_{\alpha\beta}(t)\rangle$, where $\hat{f}_1$ is the PLL's estimated fundamental frequency.

The sub-space is defined from a reference constituted by the fundamental positive sequence components on the $\alpha\beta$ reference frame:

$$\vec{u}_{\alpha\beta}(t) = \begin{bmatrix} u_\alpha(t) \\ u_\beta(t) \end{bmatrix} = \begin{bmatrix} V_1 sin(2\pi f_1 t + \phi_1) \\ V_1 sin(2\pi f_1 t + \phi_1 - \frac{\pi}{2}) \end{bmatrix}. \quad (4)$$

When the ISI-PLL correctly estimates the frequency of the input signal, that is $\hat{f}_1 = f_1$, the corresponding complex sub-space can be written in the exponential form as:

$$\begin{cases} e^{-j(2\pi\hat{f}_1 t)} = cos(2\pi\hat{f}_1 t) - jsin(2\pi\hat{f}_1 t) \\ e^{-j(2\pi\hat{f}_1 t - \frac{\pi}{2})} = cos(2\pi\hat{f}_1 t - \frac{\pi}{2}) - \\ \qquad\qquad jsin(2\pi\hat{f}_1 t - \frac{\pi}{2}) \end{cases}. \quad (5)$$

The inner products, $\vec{g}_{\alpha\beta}(t)$, of the input signals and the reference frame are calculated over a period equivalent to one cycle of the estimated signal, $T_1 = 1/\hat{f}_1$, and is given by:

$$\vec{g}_{\alpha\beta}(t) = \begin{bmatrix} g_\alpha(t) \\ g_\beta(t) \end{bmatrix} = \begin{bmatrix} \int_{T_1} v_\alpha(t) e^{-j(2\pi\hat{f}_1 t)} dt \\ \int_{T_1} v_\beta(t) e^{-j(2\pi\hat{f}_1 t - \pi/2)} dt \end{bmatrix}. \quad (6)$$

As showed in Equation 5, the complex sub-space is constituted by real and imaginary parts, thus, the inner products can also be written with real and imaginary parts, $Re\{g_{\alpha\beta}(t)\}$ and $Im\{g_{\alpha\beta}(t)\}$ respectively. The real part is explicitly calculated in Equation 7.

$$\begin{cases} Re\{g_\alpha(t)\} = \int_{t-T_1}^{t} v_\alpha(t) cos(2\pi\hat{f}_1 t) dt \\ Re\{g_\beta(t)\} = \int_{t-T_1}^{t} v_\beta(t) cos(2\pi\hat{f}_1 t - \pi/2) dt \\ \qquad\qquad = \int_{t-T_1}^{t} v_\beta(t) sin(2\pi\hat{f}_1 t) dt \end{cases}. \quad (7)$$

The imaginary part can be calculated in a similar way as seen in the original structure [21], however, the ISI-PLL estimates this component through an adaptive filter as shown in Figure 4. The input signal of this filter is given by the sum of the real parts previously calculated in Equation 7.

The structure not only estimates the imaginary part but also attenuates the components with frequency different than the fundamental one. Considering $x_\alpha = Re\{g_{\alpha\beta}(t)\}$, $\hat{x}_\alpha = Re\{g^{+1}_{\alpha\beta}(t)\}$ and $\hat{x}_\beta = Im\{g^{+1}_{\alpha\beta}(t)\}$, the following expressions in the Laplace domain can be found:

$$\begin{cases} \hat{x}_\alpha(s) = \frac{1}{s}\left[K_{FA}(x_\alpha(s) - \hat{x}_\alpha(s)) - \hat{\omega}_1 \hat{x}_\beta(s)\right] \\ \hat{x}_\beta(s) = \frac{1}{s}\left[K_{FA}(x_\beta(s) - \hat{x}_\beta(s)) - \hat{\omega}_1 \hat{x}_\alpha(s)\right] \end{cases}. \quad (8)$$

Rearranging Equation 8, the following transfer functions can be found:

$$\frac{\hat{x}_\alpha}{x_\alpha}(s) = \frac{K_{FA}(s+1)}{s^2 + s(K_{FA}+1) + K_{FA} + \hat{\omega}_1^2}, \quad (9)$$

$$\frac{\hat{x}_\beta}{x_\alpha}(s) = \frac{K_{FA}\hat{\omega}_1}{s^2 + s(K_{FA}+1) + K_{FA} + \hat{\omega}_1^2}. \quad (10)$$

The frequency responses of the transfer functions presented previously are shown in Figure 5, where the gain K_{FA} is considered to be 100. It is possible to notice how there is a large attenuation for signals with frequencies different than 60 Hz, thus, the output signals will have an enhanced immunity to harmonics distortion if compared to $Re\{g_{\alpha\beta}(t)\}$. The governing parameter for this filter is K_{FA} and by changing this value, it is possible to either increase the filtering capability to the detriment of a faster dynamic response or the other way around.

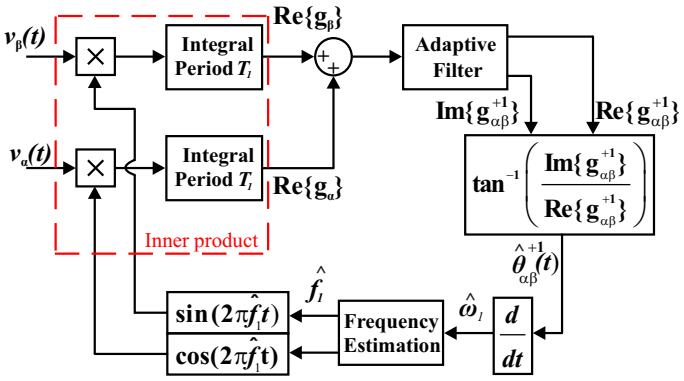

Fig. 3. ISI-PLL block diagram.

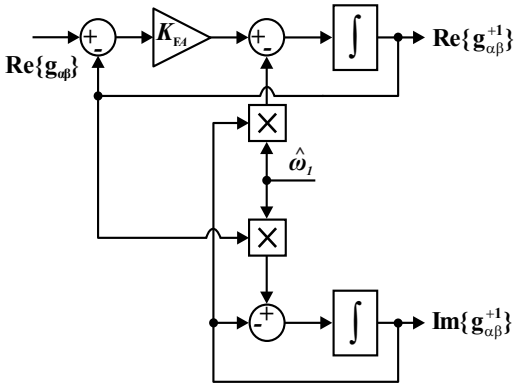

Fig. 4. Adaptive filter.

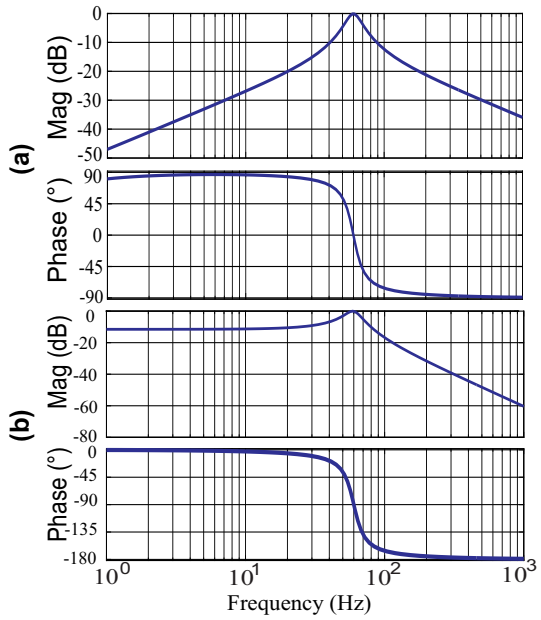

Fig. 5. Bode diagram for: (a) $\hat{x}_\alpha$ and (b) $\hat{x}_\beta$.

Having the filtered real and imaginary signals from the adaptive filter, by calculating the arctangent of the ratio between the two, one can estimate the time-varying phase-angle as shown in Equation 11.

$$\hat{\theta}^{+1}_{\alpha\beta}(t) = tan^{-1}\left(\frac{Im\{g^{+1}_{\alpha\beta}(t)\}}{Re\{g^{+1}_{\alpha\beta}(t)\}}\right) = \left(2\pi\hat{f}_1 t + \hat{\phi}^{+1}_{\alpha\beta}\right). \quad (11)$$

If the frequency is not appropriately locked with the input signal one, $\hat{f}_1 \neq f$, there will be an error defined as $\Delta f = \hat{f}_1 - f_1$. By not taking the angle from Equation 11 into account, the phase angle can be written as:

$$\hat{\theta}^{+1}_{\alpha\beta}(t) = 2\pi\hat{f}_1 t + 2\pi\Delta f t. \quad (12)$$

Differentiating both sides with respect to t, the following expression is found:

$$\Delta f = \frac{\frac{d\hat{\theta}^{+1}_{\alpha\beta}(t)}{dt} - 2\pi\hat{f}_1}{2\pi}. \quad (13)$$

As all the variables on the right side of Equation 13 are known, by integrating both sides with respect to Δt, we can find the adjustment applied to $\hat{f}_1$ over this period:

$$\hat{f}_1(t) = K_{MF}\int\left(\frac{1}{2\pi}\frac{d\theta^{+}_{1\alpha\beta}}{dt} - \hat{f}_1(t)\right)dt + f_0. \quad (14)$$

Where f_0 is defined as the initial estimated frequency (usually the nominal power frequency) for the PLL startup. K_{MF} is a gain that can either amplify or decrease the error and, therefore, speeding up or slowing down the loop's dynamic when a frequency mismatch is present.

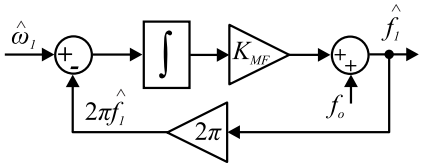

Fig. 6. Frequency estimation loop.

Lastly, in the Laplace domain, it can be noticed that the frequency loop is, in fact, a first-order low-pass filter as Equation 15 points out:

$$\frac{\hat{\omega}_1(s)}{\hat{f}_1(s)} = \frac{K_{MF}}{s + 2\pi K_{MF}}. \quad (15)$$

The ISI-PLL therefore has two filters in its structure, which greatly improves the fundamental positive sequence component estimation under faulty scenarios. The structure, however, is more complex to digitally implement than the EPLL, especially because of the inner product computation which is calculated over a period that varies according to the estimated frequency.

III. Experimental Results

A comparative analysis is made between the ISI-PLL structure and the EPLL. The EPLL parameters are defined as: $K = 300$, $K_i = 19000$ and $K_p = 300$, chosen following [20]. The ISI-PLL parameters are chosen analytically once the inner product computation makes it difficult to find a linearized model for the structure. They are defined as: $K_{FA} = 100$ and $K_{MF} = 9$. As mentioned previously, all of these parameters can easily be adjusted to improve either dynamic response or steady-state estimation precision.

The implementation is realized through the HIL (Hardware-in-the-loop) platform dSPACE 1103. To generate the input signals, the programmable power supply MX30-3Pi from California Instruments is employed. Two steady-state scenarios are considered to test the behavior of both structures under sub and inter-harmonic distortion. Dynamic state scenarios consider amplitude change, phase-angle jump and sub-harmonic distortion introduction.

A. Steady-state response

Two scenarios are considered to assess the steady-state performance of the studied PLLs. On the first scenario, alongside the fundamental component with 1 p.u. amplitude at 60 Hz frequency, there is a sub-harmonic distortion with 0.2 p.u. at 36 Hz. On the second scenario, an inter-harmonic distortion with 0.2 p.u. at 90 Hz will be added to the unitary amplitude fundamental signal. Results are shown in Figure 7, where the three-phase input signals, estimated phase-angle and estimated frequency are presented.

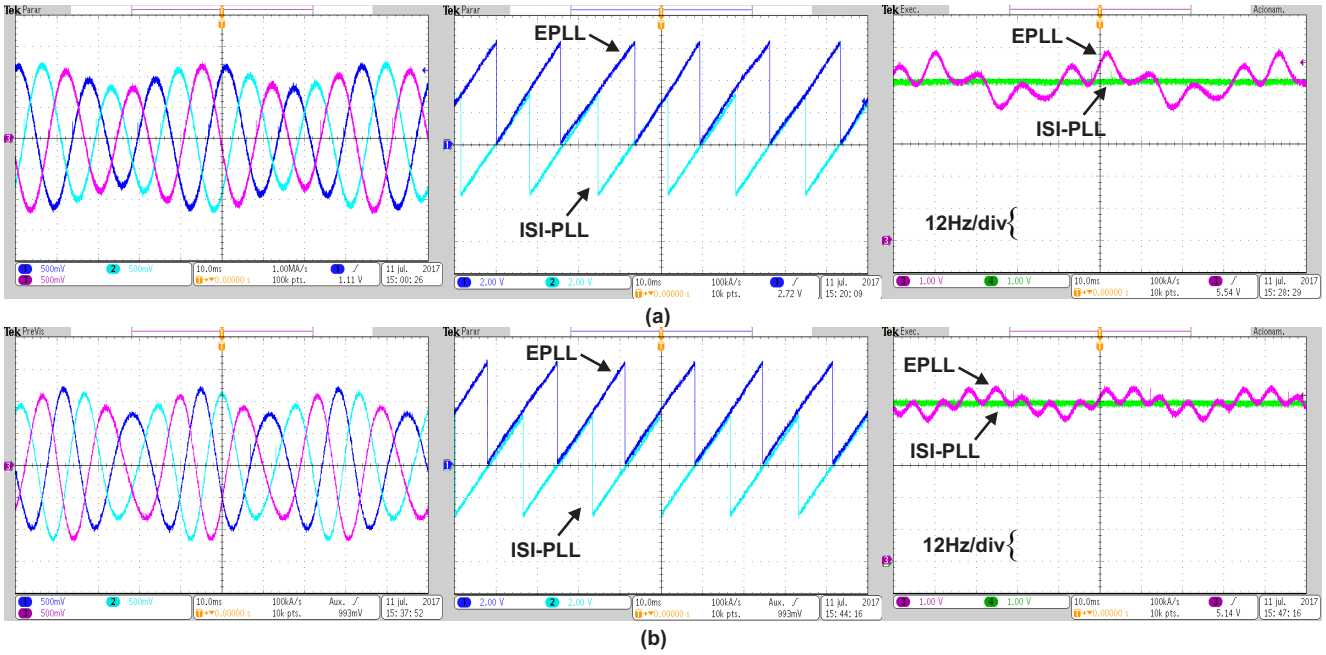

Fig. 7. Experimental evaluation of the PLLs structures under (a) sub-harmonic, (b) inter-harmonic distortion. Plots from left to right: input signals; estimated phase-angle; estimated frequency.

Figure 7(a) shows that, whereas the ISI-PLLs estimated frequency is near 60 Hz, the EPLL estimation varies and can reach values as high as 70 Hz and as low as 50 Hz. This condition has an impact on the phase-angle estimation, since this parameter is a function of the estimated frequency. This can be seen in the figure as the small oscillations on EPLLs sawtooth curve. Also, to clarify, it is important to mention that the phase-angle estimated by the EPLL varies from 0 to 2π while the ISI-PLLs varies from $-\pi$ to $+\pi$.

Figure 7(b) shows similar results to those in (a). However, in this scenario, the frequency estimated by the EPLL is more precise although a significant error can still be seen, especially if compared to the ISI-PLL estimation. The amplitude of the inter-harmonic imposed is the same as the sub-harmonic in the previous scenario, but the frequency is not as close to 60 Hz, therefore, both structures experience an improvement in accuracy.

B. Dynamic response

Three scenarios are considered to assess the dynamic performance of the structures. On the first scenario, the fundamental component has an amplitude change from 1 p.u. to 0.7 p.u.. On the second scenario, the fundamental component has a phase-angle jump of -10.8 deg. These scenarios do not involve any harmonic distortion and are meant to observe both structures transient behavior under basic parameters change. Lastly, on the third scenario, a 0.2 p.u. sub-harmonic distortion at 36 Hz is added to the fundamental component.

The input signals are represented in Figure 8 as the instantaneous aggregate voltage which is defined in [23] as: $V_\Sigma(t) = \sqrt{v_a^2(t) + v_b^2(t) + v_c^2(t)}$. If the three-phase input signal are completely balanced this curve should be seen as a constant value, whereas any unbalance or the presence of distortion will cause oscillations.

Figure 8(a) shows that, by changing the amplitude, the EPLL experiences a transient that reaches steady-state within 40 ms. Figure 8(b) shows a similar result when a phase-angle jump occurs. In both cases the ISI-PLL experience such a small change that it makes difficult to assess with the oscilloscopes chosen amplitude, however they do exist. Lastly, Figure 8(c) outputs the scenario change from when the conditions are ideal to the scenario presented previously in the steady-state sub-section.

IV. Conclusion

In this paper a performance analysis was made for the EPLL and ISI-PLL structures. The mathematical modeling of both was presented, and experimental results were obtained to verify the behavior of both for scenarios where inter-harmonics and sub-harmonics are present.

Regarding the steady-state experimental results, it is possible to notice oscillations on the estimated phase-angle curve from EPLL. This is even clearer when the estimated frequency curve is plotted. The EPLL's estimated frequency variation reaches 10 Hz whereas ISI-PLL's estimation is highly precise under the studied scenarios. The dynamic response results shown that, while ISI-PLL's estimation remain almost unchanged, the EPLL's are quite sensitive even when few changes, such as amplitude and phase-angle jump, are made. It can be concluded from the experiments that the ISI-PLL usage under sub and inter-harmonic distortions can be a very interesting option. On the other hand, compared to the EPLL,

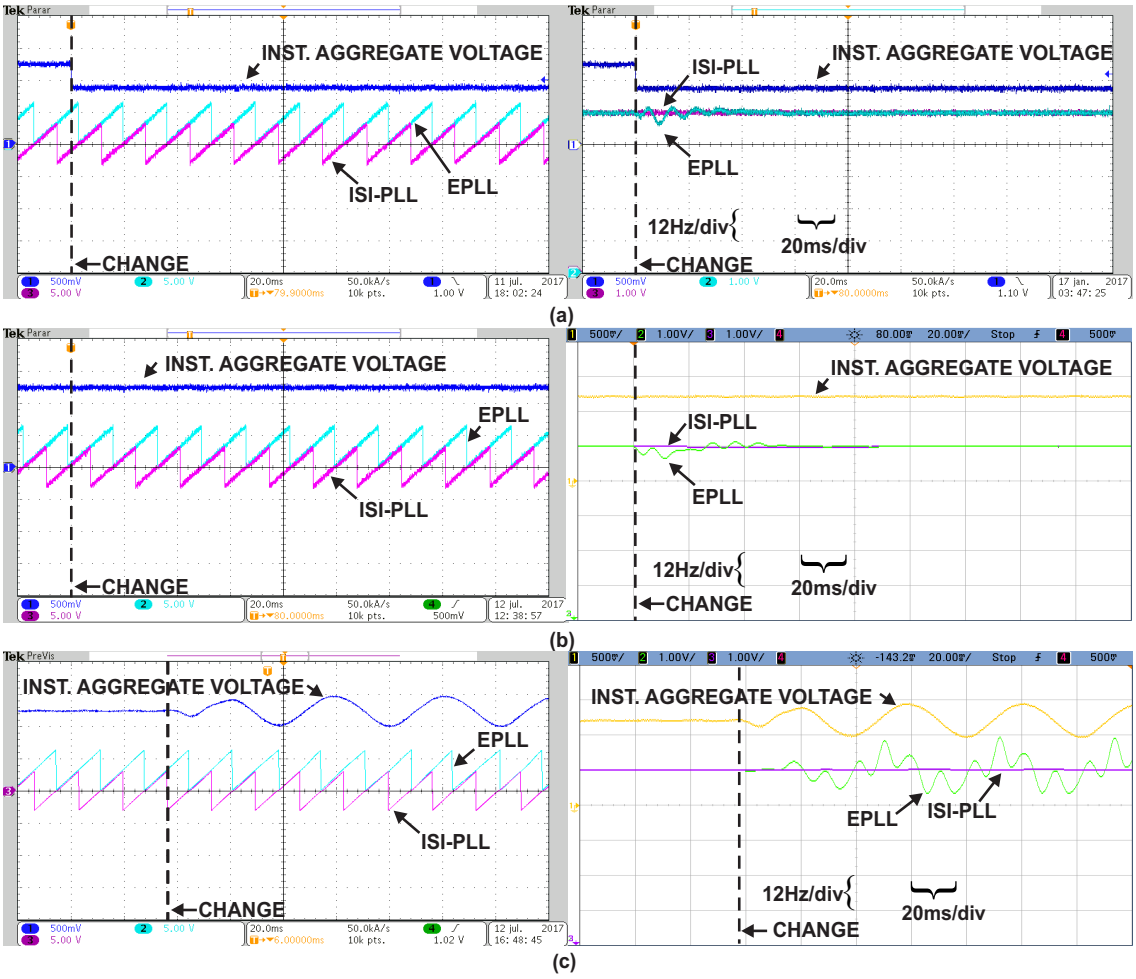

Fig. 8. Experimental evaluation of the PLLs structures under (a) amplitude change (b) phase-angle jump (c) sub-harmonic distortion introduction. Plots from left to right: estimated phase-angle; estimated frequency.

the complexity to implement the ISI-PLL algorithm is its biggest disadvantage.

ACKNOWLEDGMENT

The authors would like to thank the National Council for Scientific and Technological Development (CNPq), and Coordination for the Improvement of Higher Level Personnel (CAPES) for the financial support.

REFERENCES

[1] J. M. Carrasco, L. G. Franquelo, J. T. Bialasiewicz, E. Galvan, R. C. PortilloGuisado, M. A. M. Prats, J. I. Leon, and N. Moreno-Alfonso, "Power-electronic systems for the grid integration of renewable energy sources: A survey," *IEEE Transactions on Industrial Electronics*, vol. 53, no. 4, pp. 1002–1016, June 2006.

[2] N. G. Hingorani and L. Gyugyi, *Understanding FACTS:Concepts and Technology of Flexible AC Transmission Systems*, 1st ed. Piscataway, N.J.: Wiley-IEEE Press, 2000.

[3] C. Schauder, M. Gernhardt, E. Stacey, T. Lemak, L. Gyugyi, T. W. Cease, and A. Edris, "Development of a plusmn;100 mvar static condenser for voltage control of transmission systems," *IEEE Transactions on Power Delivery*, vol. 10, no. 3, pp. 1486–1496, Jul 1995.

[4] L. Gyugyi, C. D. Schauder, S. L. Williams, T. R. Rietman, D. R. Torgerson, and A. Edris, "The unified power flow controller: a new approach to power transmission control," *IEEE Transactions on Power Delivery*, vol. 10, no. 2, pp. 1085–1097, Apr 1995.

[5] E. H. Watanabe, R. M. Stephan, and M. Aredes, "New concepts of instantaneous active and reactive powers in electrical systems with generic loads," *IEEE Transactions on Power Delivery*, vol. 8, no. 2, pp. 697–703, Apr 1993.

[6] S. Srianthumrong and H. Akagi, "A medium-voltage transformerless ac/dc power conversion system consisting of a diode rectifier and a shunt hybrid filter," *IEEE Transactions on Industry Applications*, vol. 39, no. 3, pp. 874–882, May 2003.

[7] H. Akagi, "Active harmonic filters," *Proceedings of the IEEE*, vol. 93, no. 12, pp. 2128–2141, Dec 2005.

[8] M. Bollen, *Understanding Power Quality Problems (Voltage Sags And Interruptions)*. Standard Publishers Distributors, 2001.

[9] E. W. Gunther, "Interharmonics in power systems," in *2001 Power Engineering Society Summer Meeting. Conference Proceedings (Cat. No.01CH37262)*, vol. 2, July 2001, pp. 813–817 vol.2.

[10] E. F. da Silva, J. R. M., A. Scotti, and J. C. de Oliveira, "Power quality analysis of gas metal arc welding process operating under different drop transfer modes," in *XI Brazilian Power Electronics Conference*, Sept 2011, pp. 129–135.

[11] M. Loskarn, K. D. Tost, C. Unger, and R. Witzmann, "Mitigation of interharmonics due to large cycloconverter-fed mill drives," vol. 1, pp. 122–126 vol.1, Oct 1998.

[12] F. D. Rosa, R. Langella, A. Sollazzo, and A. Testa, "On the in-

terharmonic components generated by adjustable speed drives," *IEEE Transactions on Power Delivery*, vol. 20, no. 4, pp. 2535–2543, Oct 2005.

[13] *IEEE Recommended Practice and Requirements for Harmonic Control in Electric Power Systems*, IEEE Std. 519, June 2014.

[14] *IEEE Recommended Practice for the Analysis of Fluctuating Installations on Power Systems*, IEEE Std. 1453, Oct 2015.

[15] P. Rodriguez, A. Luna, M. Ciobotaru, R. Teodorescu, and F. Blaabjerg, "Advanced grid synchronization system for power converters under unbalanced and distorted operating conditions," in *IECON 2006 - 32nd Annual Conference on IEEE Industrial Electronics*, Nov 2006, pp. 5173–5178.

[16] P. Rodriguez, J. Pou, J. Bergas, I. Candela, R. Burgos, and D. Boroyevic, "Double synchronous reference frame pll for power converters control," in *2005 IEEE 36th Power Electronics Specialists Conference*, June 2005, pp. 1415–1421.

[17] M. Karimi-Ghartemani and M. R. Iravani, "A method for synchronization of power electronic converters in polluted and variable-frequency environments," *IEEE Transactions on Power Systems*, vol. 19, no. 3, pp. 1263–1270, Aug 2004.

[18] ——, "A new phase-locked loop (pll) system," vol. 1, pp. 421–424 vol.1, 2001.

[19] ——, "A nonlinear adaptive filter for online signal analysis in power systems: applications," *IEEE Transactions on Power Delivery*, vol. 17, no. 2, pp. 617–622, Apr 2002.

[20] M. Karimi-Ghartemani, S. A. Khajehoddin, P. Jain, and A. Bakhshai, "Comparison of two methods for addressing dc component in phase-locked loop (pll) systems," pp. 3053–3058, Sept 2011.

[21] J. A. M. Neto, L. Lovisolo, B. W. Frana, and M. Aredes, "Grid synchronization system for power converters," pp. 749–755, Sept 2009.

[22] R. G. Arajo, F. K. A. Lima, J. A. M. Neto, and C. G. C. Branco, "A phase-locked loop algorithm for single-phase grid-connected systems with sub and interharmonics immunity," in *2015 IEEE 13th Brazilian Power Electronics Conference and 1st Southern Power Electronics Conference (COBEP/SPEC)*, Nov 2015, pp. 1–6.

[23] H. Akagi, E. H. Watanabe, and M. Aredes, *Instantaneous Power Theory and Applications to Power Conditioning*. Willey-IEEE Press, 2007.